High-Resolution Genome-Wide Maps Reveal Widespread Presence of Torsional Insulation

Porter M. Hall[1], Lauren A. Mayse[1,2], Lu Bai[3,4], Marcus B. Smolka[5,6], B. Franklin Pugh[5], and Michelle D. Wang[1,2,*]

[1]Department of Physics & LASSP, Cornell University, Ithaca, NY 14853, USA

[2]Howard Hughes Medical Institute, Cornell University, Ithaca, NY 14853, USA

[3]Department of Biochemistry and Molecular Biology, Pennsylvania State University, University Park, PA 16802, USA

[4]Department of Physics, Pennsylvania State University, University Park, PA 16802, USA

[5]Department of Molecular Biology and Genetics, Cornell University, Ithaca, NY 14853, USA

[6]Weill Institute for Cell and Molecular Biology, Cornell University, Ithaca, NY 14853, USA

*Correspondence: mwang@physics.cornell.edu

Abstract

Torsional stress in chromatin plays a fundamental role in cellular functions, influencing key processes such as transcription, replication, and chromatin organization. Transcription and other processes may generate and be regulated by torsional stress. In the genome, the interplay of these processes creates complicated patterns of both positive (+) and negative (-) torsion. However, a challenge in generating an accurate torsion map is determining the zero-torsion baseline signal, which is conflated with chromatin accessibility. Here, we introduce a high-resolution method based on the intercalator trimethylpsoralen (TMP) to address this challenge. We describe a method to establish the zero-torsion baseline while preserving the chromatin state of the genome of *S. cerevisiae*. This approach enables both high-resolution mapping of accessibility and torsional stress in chromatin in the cell. Our analysis shows transcription-generated torsional domains consistent with the twin-supercoiled-domain model of transcription and suggests a role for torsional stress in recruiting topoisomerases and in regulating 3D genome architecture via cohesin. Significantly, we reveal that insulator sequence-specific transcription factors decouple torsion between divergent promoters, whereas torsion spreads between divergent promoters lacking these factors, suggesting that torsion serves as a regulatory mechanism in these regions. Although insulators are known to decouple gene expression, our finding provides a physical explanation of how such decoupling may occur. This new method provides a potential path forward for using TMP to

measure torsional stress in the genome without the confounding contribution of accessibility in chromatin.

Introduction

The double-stranded helical structure of DNA inherently results in the generation of torsional stress during a host of basic processes, including replication and transcription. Many essential motor proteins, such as RNA polymerase (RNAP), track the DNA helical groove during translocation, producing a relative rotation between the motor and the DNA. If RNAP rotation is restricted during transcription, DNA itself must twist, unwinding DNA to generate (-) supercoiling behind the polymerase, while overwinding DNA to generate (+) supercoiling in front, as described by the twin-supercoiled domain model of transcription[1–6]. Excessive torsional stress generated during transcription may, in turn, present challenges to motor progression[2,3,5–7]. Topoisomerases, a class of enzymes that can relax torsional stress and alter DNA topology, are essential to ensure cell cycle progression and are required for efficient transcription to occur[8–14]. However, residual supercoiling may offer advantages to cell survival. For example, (-) torsional stress behind these rotary motors may slow motor progression[2,3,14] while promoting processes that require DNA unwinding, such as transcription initiation, replication, or DNA repair[6,15–20]. (+) torsional stress in front of these rotary motors, on the other hand, may slow motor progress[2,3,14,21], dissociate proteins ahead of advancing motors[22] and promote genome organization[23–25].

Importantly, torsion can act over a distance so that torsion generated from one gene can regulate the transcription of a neighboring gene. For divergent genes, (-) torsion generated from the transcription of one gene can facilitate DNA unwinding of the promoter of the neighboring gene and thus promote its expression[5,6,26]. Interestingly, some promoter architectural factors, including sequence-specific transcription factors (ssTFs), can decouple the transcription between neighboring genes, effectively acting as insulators[27,28]. Although the precise mechanism of insulation remains unclear, it raises the possibility that ssTFs can insulate torsion between neighboring genes. Addressing such questions requires sensitive techniques to investigate torsional stress across the genome *in vivo*.

Elucidating the impact of torsional stress in cells requires accurate mapping of torsion. This requires a sensor that ideally should interact with the DNA to report its torsional stress, have fast and tunable binding kinetics for capturing a snapshot of the cellular state, be readily delivered into the cell, and have a robust readout. These requirements are nearly all met by

66 4,5′,8-trimethylpsoralen (TMP), a small photoreactive DNA intercalator that can cross-link to
67 DNA upon UVA irradiation, with the extent of cross-linking modulated by TMP concentration
68 and UVA dosage[29]. Because TMP unwinds DNA upon intercalation, its binding affinity, and thus
69 the probability of generating interstrand crosslinks (ICLs) at a given site, is influenced by local
70 torsional stress. Previous studies suggest that the relationship between torsion and the
71 crosslinking rate is approximately linear across a relevant range of torsional stress[30,31]. While
72 psoralen shows great promise for mapping torsional stress, significant challenges remain to be
73 addressed before its full utilization can be realized.

74 Previous studies have laid the foundation for using TMP and other psoralen derivatives
75 as torsional sensors[30,32–35]. However, factors besides the torsional state influence the resulting
76 photo-binding distribution[30]. Importantly, the torsion signal mapped using TMP contains a zero-
77 torsion baseline that varies across the genome, and this baseline is dependent on DNA
78 sequence and TMP accessibility. Establishing this baseline is crucial for differentiating between
79 (-) torsion and (+) torsion states across the genome, and in the absence of the zero-torsion
80 baseline, the contribution from torsion to TMP intercalation may be conflated with TMP
81 accessibility[36]. However, it is challenging to establish such a baseline as experiments must be
82 performed under conditions that preserve both the chromatin state and the binding states of
83 other proteins. Thus, interpreting the psoralen sensor readout requires a method to establish
84 the zero-torsion distribution, but such methods have yet to be firmly established.

85 The impact of underlying DNA sequence on the zero-torsion psoralen binding landscape
86 has been previously addressed by comparing the results from psoralen photo-binding in the cell
87 to that of purified genomic DNA[30,32,33,35,36]. While this method corrects for the intercalation
88 sequence-dependence, it does not account for the reduction of photo-binding due to restricted
89 accessibility caused by bound proteins or chromatin. Indeed, previous studies have shown that
90 chromatin reduces global psoralen crosslinking, suggesting that local effects of accessibility may
91 be even more pronounced[30]. One method to assess the zero-torsion baseline is to digest the
92 DNA using a DNA-nicking enzyme[34]. Still, this approach cannot ensure the preservation of the
93 DNA or chromatin state before psoralen photo-binding. Other methods modulate RNAP or
94 topoisomerase activities to generate a comparative map of torsional stress to extrapolate what
95 might be a zero-torsion state but do not solve the problem at its core[32–35]. Importantly,
96 alteration of normal cellular functioning can, in turn, alter DNA accessibility or the zero-torsion
97 state. These complications give a clear motive for devising a strategy of measuring the zero-
98 torsion baseline of TMP to reveal a more accurate signal of torsional stress.

To directly address this limitation, we report a method that enables psoralen mapping on relaxed DNA *in situ* while preserving the chromatin state at high resolution. We demonstrate the application of this method using *S. cerevisiae,* but the method is generalizable to other organisms. We found that the zero-torsion baseline contains significant contributions from individual nucleosomes within genes. After removing this baseline, we obtained a torsion signal that identifies regions of the genome under (-) torsion or (+) torsion. This revealed the twin-supercoiled domain model of transcription and allowed examination of how torsion may facilitate the recruitment of topoisomerases. We also show direct evidence for the presence of (+) torsion at cohesin-mediated loop boundaries, implicating its role in loop anchoring. Finally, we show evidence that sequence-specific transcription factor (ssTF) insulators prevent crosstalk between divergent promoters, providing a possible explanation for transcriptional coupling between promoters that lack bound insulators. This method provides a potential path forward for measuring torsional stress using psoralen-based methods in any cellular context.

Results

A method to establish the zero-torsion baseline

To establish the zero-torsion baseline for the psoralen signal, we must establish a method to account for psoralen's sequence preference and accessibility without torsion under conditions that preserve the native-bound protein landscape (Fig. Supplement 1). To do this, we developed a method to prepare the chromatin zero-torsion state *in situ* and applied psoralen photo-binding (Fig. 1a, right panel). Formaldehyde preserved the chromatin landscape and transiently bound proteins (Materials and Methods) while stopping any subsequent cellular processes. The fixed cells were permeabilized so enzymes could diffuse into the nucleus. For *S. cerevisiae*, the cell wall was gently digested to create spheroplasts. To release torsion in intact spheroplast nuclei, we utilized DpnII, chosen for its high cut site density but inability to processively digest DNA, thus maintaining psoralen's crosslinking ability. Upon DNA digestion, we observed an average fragment size of ~2 kb, sufficiently short to release torsion but long enough to provide a chromatin substrate for psoralen binding. This zero-torsion state preparation was subsequently crosslinked using 365-nm light, enabling measurement of the torsion-free TMP intercalation landscape (referred to as TMP signal without torsion). The *in vivo* measurement (TMP signal with torsion) was performed by directly adding TMP to the yeast media since unmodified TMP is cell-wall permeable. Cell permeability enables photo-crosslinking to be performed before cells are harvested, thus capturing native cell activity (Fig. 1a, left panel).

133 To locate psoralen crosslinks on the DNA, we utilized an exonuclease-based enrichment
134 strategy followed by an Illumina-compatible library prep, similar to TMP-seq[30,33]. Exonuclease-
135 based enrichment relies on interstrand crosslink (ICL) formation, which prevents DNA
136 denaturation before digestion by the single-strand-specific ExoI. We use the digested fraction
137 to estimate the crosslinking density and provide quality control for ICL enrichment over
138 the background. As controls, we found that libraries prepared without psoralen photo-binding
139 showed a very low signal level (Fig. Supplement 2). By tuning the UV dosage, we ensured that
140 the average densities of the *in vivo* and zero-torsion measurements were comparable at ~0.1-
141 0.25 ICLs/kb (Fig. Supplement 2). If ICL density is too low, the signal-to-noise ratio is poor; if ICL
142 density is too high, there can be library preparation artifacts (Fig. Supplement 3). ICL densities
143 within the range used display remarkably similar signals (Fig. Supplement 2). This allows the
144 TMP signals with and without torsion to be compared to obtain an accurate genomic map of
145 psoralen binding due to torsional stress. In addition, we conducted a control experiment using
146 purified DNA to assess the extent of psoralen crosslinking due to DNA sequence preference (Fig.
147 Supplement 2). This TMP signal was only used during an intermediate analysis step to isolate
148 the psoralen intercalation preference not due to DNA sequence (Fig. 1b,c).

149 **TMP allows the mapping of positioned nucleosomes**

150 To evaluate the contributions of DNA accessibility to the TMP intercalation profile, we
151 examined the TMP signal downstream of transcription start sites (TSSs), which are known to
152 have positioned nucleosomes[37,38]. We expect TMP to preferentially intercalate in linker DNA
153 regions between nucleosomes in samples with and without torsion, and the ability to reveal
154 these well-positioned nucleosomes is a measure of our TMP data quality. We found a striking
155 similarity between the signals from the two samples (Fig. 1b). This finding demonstrated that
156 the *in vivo* psoralen signal is likely dominated by accessibility so that TMP intercalation
157 preference due to torsion may represent a smaller contribution to the overall signal than
158 protein-mediated DNA accessibility. Therefore, using the TMP intercalation signal alone to
159 indicate torsion may be prone to interpretation artifacts.

160 For both datasets, we detected a TMP peak upstream of the TSSs, with the peak
161 amplitude being slightly larger for the condition with torsion. This peak coincides with the
162 nucleosome-free regions (NFRs), which should be more accessible to TMP (Fig. 1c). Within the
163 gene bodies, we also observed a clear ~160 bp periodic signal, similar to that of the positioned
164 nucleosomes near the promoters (Fig. 1c). However, the periodic pattern anti-correlates with
165 H3-ChIP-MNase seq data, indicating that psoralen prefers to bind in the linker regions between
166 nucleosomes or in NFRs (Fig. 1c)[27]. The decay in the amplitude of the somewhat sinusoidal TMP

167 signal away from the TSS mirrors the decay in the amplitude of the H3-ChIP-seq signal,
168 reflecting a decrease in nucleosome phasing further from the promoters[38]. Immediately
169 downstream of the transcription end sites (TESs), we observed a smaller TMP peak than before
170 the TSSs, likely due to the presence of promoter regions associated with a downstream
171 codirectional gene. These findings show that the TMP intercalation distribution reflects many
172 features previously observed using other chromatin accessibility assays and suggest that the
173 TMP signal may be dominated by chromatin accessibility.

174 **Twin-supercoiled domains of transcription**

175 To determine psoralen intercalation due to DNA torsion, we subtracted the zero-torsion
176 baseline from the *in vivo* distribution, eliminating contributions from sequence preference and
177 accessibility (Fig. 2a,b). The resulting signal has a ~ 5-fold reduced peak-to-valley amplitude and
178 should reflect contributions solely due to torsional stress. Most of the nucleosome signal was
179 abolished within the gene bodies, indicating that most accessibility bias has been removed,
180 although a small residual remained (Fig. 2b). We refer to the corrected signal as the "torsion
181 signal," with a positive value indicating (-) torsion, which facilitates psoralen intercalation, and a
182 negative value indicating (+) torsion, which restricts psoralen intercalation. Using this approach,
183 we examined whether we could detect the torsional state more accurately during transcription.
184 To examine the torsion distribution along a gene, we focused on regions near promoters and
185 terminators. We found the torsion signal now reveals (-) torsion upstream of promoters and (+)
186 torsion downstream of terminators (Fig. 2b). This may be interpreted as a statistical average of
187 a bulk population of Pol II molecules, which have elongated to random locations along the gene
188 in different cells. Since each Pol II molecule generates (-) torsion behind and (+) torsion ahead,
189 according to the twin-supercoiled-domain model, the net torsion signal from different Pol II
190 molecules averages to near zero, except at gene boundaries. We also found that torsion is
191 confined to within 1-2 kbp of the promoters and terminators, supporting previous findings that
192 transcription-dependent dynamic supercoiling is a short-range genomic force[32].

193 To further examine whether the torsion signal is due to transcription, we classified
194 genes into percentile groups based on their expression level (Fig. 2c,d). We expected that the
195 average transcription-generated torsional stress should increase with increased gene
196 expression. Thus, we sorted the genes based on their expression level according to previous
197 mRNA-seq data[39]. Consistent with this prediction, genes in the bottom 20% of the expression
198 level do not display a significant peak near the promoters nor a significant valley near the
199 terminators. As the gene expression level increases, the torsion signal amplitudes near the
200 promoters and terminators monotonically increase on average (Fig. 2c,d). As expected, gene

201 expression strongly correlated with Pol II presence along the genes (based on previous ChIP-seq
202 data of Pol II[27]). This shows that active transcription accumulates torsional stress near highly
203 transcribed genes, supporting earlier findings from *in vitro* and *in vivo* studies[2,4–7,40–42].

204 The persistence of torsion near genes, even with full native topoisomerases, indicates
205 that topoisomerases cannot fully keep up with transcription activities. To examine the
206 correlation of torsional stress with topoisomerase activity, we analyzed previous ChIP-seq data
207 of topoisomerase I (topo I) and topoisomerase II (topo II)[27], which are the primary enzymes for
208 relaxing transcription-generated torsion. Topo I binds near promoters and terminators, and its
209 enrichment level correlates with an increase in the torsion signal (Fig. 2c). In contrast, topo II
210 binds near promoters but not near terminators. As the torsion signal increases, the topo I and
211 topo II enrichment levels also increase, suggesting that torsion might facilitate topoisomerase
212 recruitment or retention. Unlike topo I, which binds to one DNA segment, topo II relaxes DNA
213 via a strand-passage mechanism[43] and has been found to prefer binding to a DNA
214 crossover[13,44–47]. Because the DNA in a nucleosome wraps around the histone octamer in a left-
215 handed fashion, the nucleosome conformation exhibits a chiral response to DNA
216 supercoiling[48,49]. While (-) torsion readily enables DNA crossing formation via the juxtaposition
217 of the entry and exit DNA segments in a nucleosome, (+) torsion displaces entry and exit DNA
218 segments before bringing them together again, buffering torsional stress[14,48]. Thus, there is less
219 DNA crossing at a nucleosome available to allow topo II binding. Consistent with this
220 interpretation, we previously found that topo II has a faster relaxation rate and is more
221 processive on chromatin under (-) supercoiling than under (+) supercoiling[44]. Thus, the absence
222 of topo II near the terminators may not be due to any active exclusion of topo II at those
223 regions but is a natural consequence of the interplay between the DNA chirality and
224 nucleosome chirality.

225 Previous studies suggest torsion accumulates more significantly over longer genes[5]. As
226 Pol II elongates, its rotation may be more restricted with a lengthening in the RNA transcript,
227 which is known to be associated with large machinery, such as spliceosomes[50]. Thus, torsional
228 stress might significantly increase toward transcription termination for longer genes. We
229 grouped data based on gene size (Fig. 2c,d), and consistent with this prediction, the (-) torsion
230 near the promoters remained unchanged with an increase in gene size, but the (+) torsion near
231 the terminators increased with gene size to a moderate extent. As expected, we found no
232 significant dependence of topo I or topo II enrichment on gene size near the promoters.
233 However, we noticed a similar lack of dependence near the terminators, likely due to the
234 moderate dependence of torsion on gene size.

235 **Torsion accumulation between genes**

236 Transcription-generated torsion may dissipate over distance due to topoisomerase
237 relaxation and DNA end rotation[6,32,51]. If so, torsion generated from one gene will most likely
238 impact the torsional state of neighboring genes. For example, (-) torsion may more likely
239 accumulate near promoters of two divergent genes, while (+) torsion may more likely
240 accumulate near terminators of two convergent genes. To examine this prediction, we plotted
241 the torsion signal in three gene-pair configurations (Fig. 3). We mapped the average behavior of
242 torsional stress in the intergenic regions after rescaling the intergenic distance between nearest
243 neighbors. We found that between promoters of two divergent genes, the torsion signal rises
244 throughout the intergenic region, consistent with (-) torsion accumulation between these gene
245 pairs. Conversely, we observed that between terminators of converging genes, the torsion
246 signal drops throughout the intergenic region, consistent with (+) torsion accumulation
247 between these gene pairs. When two neighboring genes are oriented codirectionally, the
248 torsion signal drops after the terminator of the trailing gene and rises before the promoter of
249 the leading gene, consistent with generation of (+) torsion by the trailing gene followed by
250 generation of (-) torsion by the leading gene. Thus, by grouping neighboring genes in these
251 configurations, we demonstrate how torsion accumulates between neighboring gene pairs.

252 Since transcription-generated torsional stress hinders Pol II progression, topoisomerases
253 must be recruited to active genes to resolve the torsional stress. To examine where Pol II, topo
254 I, and topo II are located, we analyzed previous ChIP-seq data of Pol II, topo I, and topo II[27]. We
255 show that Pol II has a minimal presence in the intergenic region between divergent genes and is
256 enriched in the intergenic region between convergent genes, consistent with a previous finding
257 that after termination, Pol II tends to remain on the DNA downstream of the terminator[27,39].
258 We also find that topo I is enriched in all intergenic regions with significant (+) torsion or (-)
259 torsion, indicating that topo I effectively targets regions under torsional stress. In contrast, topo
260 II localizes to the intergenic region between divergent genes but is depleted from the intergenic
261 region between convergent genes, indicating that topo II prefers regions with (-) supercoiling
262 but is restricted from regions with (+) supercoiling, further supporting our interpretations
263 above. These data further demonstrate how topo I and topo II may differentially target diverse
264 environments in the genome.

265 **The role of torsion in genome structure**

266 Maintenance of three-dimensional genome structure is a crucial step in cellular
267 function. Recent yeast genome studies have found mitotic loops near the boundaries of
268 convergently oriented gene pairs[23,24,52]. This suggests that (+) torsional stress may regulate

genome folding. We examined the signal near loop boundaries (Fig. 4a) by aligning all loop boundaries and grouped signals based on the looping strength of previously published MicroC-XL Data[52]. This sorting method showed that cohesin[24] is enriched at the two-loop boundaries as expected. Using this sorting method, we found (+) torsion signal at the loop boundaries, which also coincide with regions of convergent gene pairs. We found that (+) torsion correlates with strengthening cohesin loop boundaries, suggesting that (+) torsion in these regions may facilitate cohesin recruitment (Fig. 4a, cartoon). These data provide evidence that the (+) supercoiling generated by transcription may facilitate genome folding in coordination with other participating proteins.

Insulators decouple torsion between divergent genes

While a single (+) torsion intergenic region is present between two convergent genes, we detect two (-) torsion intergenic regions between two divergent genes (Fig. 3). The presence of the two (-) torsion peaks indicates that (-) torsion from these promoters is somewhat decoupled. However, it is unclear what limits the diffusion of (-) torsion between the two promoters. Thus, we systematically examined the promoter regions of different promoter architectures to identify factors that may play a role.

Most promoters in *S. cerevisiae* are not regulated by ssTFs and thus unbound by anything besides a PIC (termed "UNB")[27,53]. Interestingly, our data show a single elevated (-) torsion region between this UNB class of divergent promoters (Fig 4b, upper and middle plots), suggesting that torsion generated from one gene can impact the expression of its neighboring gene, consistent with previous findings that the expression of these genes is coupled[27,53]. Another large class of *S. cerevisiae* promoters (termed "TFO") are regulated by insulator ssTFs, such as Reb1 and Abf1, which decouple interactions between neighboring genes[27,28,53–55]. A minority of genes, such as inducible promoters (termed "STM"), are even more highly regulated by a host of additional transcription factors and usually contain an upstream activating sequence[27]. Strikingly, these bound promoters show two distinct (-) torsion peaks, suggesting that the insulators can insulate torsion between the two genes (Fig 4b, upper and lower plots). This result indicates that bound insulators may be anchored to cellular structures in a manner that prevents rotation of the bound DNA segments and thus blocks the progression of torsion from one promoter to the next. Given that DNA unwinding facilitates transcription initiation, insulators may prevent torsional crosstalk between adjacent divergent promoters while also preventing TATA-binding protein (TBP) from sliding back and forth between promoters.

302 ## Discussion

303 This work developed a method to profile the *in situ* zero-torsion baseline of psoralen-
304 based mapping of torsional stress in yeast. The approach enabled high-resolution mapping of
305 the psoralen intercalation distribution on torsionally relaxed DNA, while preserving the protein-
306 bound state of chromatin. This preservation is crucial to correcting the psoralen-based torsion
307 map because it allows the removal of the contributions of both chromatin accessibility and DNA
308 sequence. Through this process, we found that the psoralen technique is excellent at
309 generating high-resolution accessibility maps of chromatin, resolving positioned nucleosomes
310 at a resolution superior to that of ATAC seq[56]. This demonstrates the potential utility of
311 psoralen well beyond torsional measurements.

312 Our resulting torsion signal also reveals a characteristic torsion distribution of the twin-
313 supercoiled-domain model of transcription with (-) torsion behind promoters and (+) torsion in
314 front of terminators. We demonstrate how torsion increases with gene expression, and
315 topoisomerases are recruited to regions with torsion. We also provide an explanation for the
316 differential enrichment of topo I and topo II based on the torsional mechanics of chromatin. In
317 addition, we show that cohesin loop boundaries coincide with regions of (+) torsion in the
318 genome, indicating a role of torsion in helping cohesin restructure the genome topology.
319 Importantly, we provide a possible physical explanation for how ssTF insulators may decouple
320 highly regulated divergent genes and insulate gene expression. We show that (-) torsion
321 diffuses across promoter regions lacking ssTFs, while (-) torsion is restricted to their respective
322 promoters in the presence of ssTFs. These findings suggest that these ssTFs may insulate
323 torsion between the promoters to decouple their expression.

324 Accessibility is likely to greatly influence the readout of any torsion sensor that relies on
325 DNA binding. Thus, establishing the zero-torsion baseline is an essential step and must be
326 performed under a condition that keeps chromatin intact. While torsion sensors other than
327 TMP have been applied to generate genomic maps, these sensors, such as biotin-functionalized
328 psoralen derivatives[34–36] and the bacterial protein GapR[57], are larger in size than TMP, and thus,
329 these sensors are likely also sensitive to DNA accessibility. Since the method we developed to
330 obtain the zero-torsion state is not specific to any sensor, it may be applied to other torsion
331 sensors. Additionally, although this study utilized budding yeast as a model organism,
332 preparation of the zero-torsion state can be similarly applied to cells of other organisms. Our
333 work shows a way to measure torsion more accurately and helps to lay a foundation for future
334 quantitative studies of torsion in the genome.

335

Materials and Methods

Cell Culture

The *Saccharomyces cerevisiae* strain BY4741 (*MAT a his3Δ1 leu2Δ0 met15Δ0 ura3Δ0 bar1::NatMX* his3Δ1::HIS3-ADH1pr-hENT-GPDpr-HSV-TK)[58] was used for all experiments. Cells were grown at 30°C in YPD media until the OD600 reached ~0.6, and then processed for different conditions as described below.

Zero torsion state preparation

Cells designated as zero torsion state controls were crosslinked with 1% (v/v) formaldehyde (Fisher, F79-500) for 15 minutes at 30°C. Formaldehyde was quenched with 0.4 M glycine (Sigma, 357002) for 5 minutes at room temperature. Following quenching, cells were pelleted and washed 2X with PBS at 4˚C. Next, cells were spheroplasted via 0.01% (v/v) 10 mg/µl zymolyase (Sunrise Science Products, N0766391) treatment in 1 M sorbitol (Sigma, S6021), 0.5 mM 2-mercaptoethanol (Sigma, 444203) for 20 minutes. Spheroplasts were confirmed to be >90% of cells using microscopy. Formaldehyde-fixed spheroplasts were centrifuged at 1,000 g for 10 minutes at 4˚C, washed with 25 ml of cold PBS (Thermo, AM9624), and resuspended in 100 µl of 1x DpnII reaction buffer (NEB, R0543) containing 100 units of DpnII (NEB, R0543) and supplemented with 0.1% (v/v) NP-40 (Thermo, 85124), and 10 µM TMP (Sigma, T6137). Samples were incubated for 2 hours at 37°C followed by TMP photobinding as described below.

Trimethylpsoralen Photobinding

The 4,5', 8-trimethylpsoralen (TMP) was dissolved in 100% ethanol at a final stock solution of 2 mM. TMP was added to growing cells at a final concentration of 10 µM and cells were further incubated at 30°C for 1 hour. Twenty-five mL of cell solution was placed in a 10 cm petri dish and exposed to ~0.15 W/cm^2 of 365-nm light for 20 seconds. Directly after TMP photobinding, the cells were fixed in 95 ml 70% -20 °C ethanol and placed at -20°C overnight. Cells were then harvested by centrifugation at 10,000 g for 10 minutes, resuspended in 500 µl of 50 mM sodium citrate (Sigma, 567446), pH 7.4, and incubated at room temp for 10 minutes. Centrifugation and wash steps were repeated once more, followed by a 20-minute Zymolyase treatment as detailed above. Spheroplasts were harvested by centrifugation and resuspended in 100 µl of lysis buffer (300 mM NaCl (Fisher, BP358), 50 mM EDTA (Fisher, AM9260G), 2% SDS (Sigma, 71725), and 5 % (v/v) RNase A (Thermo , 12091021) for ~2 hours and then vortexed for 2 minutes. 10 µl of Proteinase K (NEB, P8107S) was added, and cells were incubated for 2 hours at 65 °C.

Zero torsion samples followed a similar photobinding protocol but were exposed to UV light at ~0.35 W/cm^2 for 10 seconds in a 1.5 ml Eppendorf tube. Samples were harvested at 10,000 g at 4°C, the supernatant was removed, and they were resuspended in 100 µl of Lysis buffer containing 10 µl Proteinase K. The zero torsion samples were incubated at 65°C

373 overnight to reverse formaldehyde crosslinks. After lysis, genomic DNA was extracted from all
374 samples via 2X phenol-chloroform (Sigma, 77617) extraction followed by isopropanol (Sigma,
375 59304) precipitation.

376 **TMP-seq**

377 The TMP-seq protocol was adapted from previous work[30,33]. Extracted genomic DNA
378 was sonicated to ~400 bp fragments using appropriate settings on a Covaris E200 sonicator.
379 Following sonication, DNA was treated with 5 µl RNase A and purified using a Zymoclean DNA
380 Clean and Concentrator-5 kit according to the manufacturer's protocol using a 7:1 binding
381 buffer:sample ratio. After quantification using a Biotum HS DNA quantification kit, 250 ng of
382 DNA was diluted into 86 µl of 10 mM Tris-Cl pH 8.5, incubated at 98°C for 15 minutes, and then
383 directly moved to ice for 2 minutes. DNA was then digested with 4 µl of ExoI (NEB, M0293) in 1X
384 ExoI reaction buffer at 37°C for 1 hour. This digestion process was repeated by incubating at
385 98°C for 1 hour and then adding an additional 4 µl of ExoI followed by another incubation at
386 37°C for 1 hour. Digested samples were purified using a Zymo DNA Clean and Concentrator-5
387 kit using a 7:1 binding buffer: sample ratio. DNA was again quantified using the Biotum HS DNA
388 assay. Illumina adaptors were ligated to the digested samples using the NEBNext Ultra II DNA
389 library prep kit for Illumina (NEB, E7645) at half the standard total reaction volume of the
390 manufacturer's protocol. Adapter ligated DNA was purified with 2X Ampure beads (Beckman
391 Coulter) and eluted in 40 µl of 10 mM Tris-Cl pH 8.5. DNA was stored at -20 C until further
392 processing.

393 To locate psoralen interstrand crosslinks, DNA from the previous step was incubated
394 with 5 µl of lambda exonuclease (NEB, M0262) in the provided buffer in a 50 µl total reaction
395 volume at 37°C for 1 hour, purified with 1.8X Ampure beads, and eluted with 30 µl of 10 mM
396 Tris pH 8.5. Lambda-digested DNA was then subjected to 10 rounds of primer extension with
397 Q5 DNA polymerase (NEB, M0491), using 10 nM of the primer (ID): 5'-
398 GTGACTGGAGTTCAGACGTGTGCTCTTCCGATC*T on a thermocycler (98°C for 10s → 10 rounds
399 (98°C, 10s → 65°C, 2 min)→ 65°C, 5min → 95°C 1min → 4°C). Products were purified using 1.8x
400 Ampure beads and eluted in 40 µl 10mM Tris pH 8.5. Primer extension products were ribotailed
401 using 1.4 µl Terminal Transferase (NEB, M0315) and 0.4 mM rGTP (Roche, 11277057001) in
402 Terminal Transferase buffer supplemented with 0.25 mM $CoCl_2$ by incubating at 37°C for 30
403 minutes followed by incubation at 75°C for 20 min. Ribotailed products were purified with 1.8X
404 Ampure beads, eluted with 30 µl 10mM Tris pH 8.5. Purified ribotailed products were ligated
405 with 0.33 µM annealed adapter oligos (IDT) (Top: 5'p-AGA TCG GAA GAG CGT CGT GTA GGG
406 AAA GAG TGT-3', Bottom: 5' ACA CTC TTT CCC TAC ACG ACG CTC TTC CGA TCT CCC -3') using 1.2
407 µl T4 DNA ligase (NEB, M0202S) in the provided buffer for 1 hour at 16 °C, and subsequently
408 purified with 1.8X Ampure beads and eluted in 20 µl 10mM Tris pH 8.5. Finally, products were
409 indexed and amplified using NEBNEXT Multiplex Oligos for Illumina set 1 (NEB, E7600) following
410 the manufacturers protocol with a total of 12 PCR cycles. The PCR products were purified using

411 0.8X Ampure beads and eluted in TE (Invitrogen). Samples were pooled at equimolar
412 concentrations and empty adapters were removed from the pool.

413 **Sequencing and Data Processing**

414 Pooled libraries were sequenced on a NextSeq 2000 (Illumina) using a NextSeq 2K P2
415 100 bp kit (Illumina) in paired-end mode with a 63 bp Read_1 and 59 bp Read_2. Sequencing,
416 demultiplexing and Fastq generation were performed by the Cornell Biotechnology Resource
417 Center. Fastq files were aligned to the SacCer3 Genome using BWA-mem2[59] with default
418 settings for paired-end reads. Sam files were converted to BAM files followed by fixmate and
419 duplicate marking using Samtools[60]. Duplicates were again marked using picard-
420 MarkDuplicates[61], and duplicates were removed using Samtools-view. Bedgraph files were
421 generated using deeptools[62] bamCoverage with 10 bp bins using the following settings (--
422 samFlagInclude 64 --Offset 1) yielding the coverage of the 5' end of Read_1 where the ICL was
423 located.

424 Bedgraph files were further processed in MATLAB to ensure one bin per 10 bp interval,
425 and normalized to the mean number of reads per bin. Replicate bedgraphs were averaged, and
426 indicated subtractions were done using MATLAB. Normalized bedgraphs were converted to
427 bigwig files using ucsc-bedGraphToBigWig[63]. Heatmaps and composite plots were generated
428 using deeptools computeMatrix, and visualized using Origin Lab. Bed files containing
429 coordinates of verified *s. cerevisiae* ORFs were downloaded from the Saccharomyces Genome
430 Database (SGD)[64,65], and a region blacklist was downloaded from the yeastepigenome.org[27].
431 Bed files for each gene configuration in Figure 3 were generated by considering the boundaries
432 of nearest neighbor verified ORFs and classifying them based on their strand configuration.
433 Regions that had any annotations according to the list of all yeast genes from the SGD were
434 removed to isolate true intergenic regions. The resulting Bed files were used to make
435 heatmaps and composite plots as described above.

436 **Data Processing**

437 BAM files of ChIP-Exo, and H3-ChIP-MNase data was downloaded from
438 yeastepigenome.org[27]. For ChIP exo, bigwig files were calculated using the 5' end of read 1 as
439 in[27]. Signals were then normalized to the mean number of reads per 10bp bin. For H3-ChIP-
440 MNase, the center of the fragment was considered. Top1 and Top2 ChIP-Exo data were further
441 processed by subtracting the No-TAP control (ChIP-Exo background). Previous Scc1 ChIP-seq IP
442 and Input DNA data was processed by downloading bigwig files from GSE235560[24]. Deeptools
443 bigwigCompare was used to normalize Scc1 ChIP/Input DNA.

444 mRNA-seq data was downloaded from GSE76142[39] in bigwig format. The minus strand
445 signal was subtracted from the plus strand signal. Expression level for a gene was calculated
446 using mean absolute value of the subtracted signal within the ORF, bed files containing
447 expression levels were used to separate data into percentile groups.

To determine positions of intrachromosomal loop boundaries and their scores, mcool files of MicroC-XL data were downloaded from GSE151553[52]. Boundaries were located and scored using cooltools dots[66] with a 500 bp bin size. Loop calls were refined by only considering the smallest loops in nested configurations, thereby only representing each region once. Boundary positions were adjusted by locating the position of the nearest (<500 bp) Scc1-ChIP-seq peak on either loop boundary.

Data and Material Availability

Raw and processed sequencing data files have been deposited to GEO under accession GSE284352. The custom code used to process the raw data and generate plots is available on GitHub (https://github.com/WangLabCornell/Hall_et_al).

Acknowledgments

We thank members of the Wang Laboratory for helpful discussion and comments and the Cornell Biotechnology Resource Center for sequencing support. This work is supported by the National Institutes of Health grants R01GM136894 (to M.D.W.), T32GM008267 (to M.D.W.), and R35GM145217 (to B.F.P.). M.D.W. is a Howard Hughes Medical Institute investigator.

Additional Information

Contributions

Conceptualization, P.M.H and M.D.W; Methodology, P.M.H, L.B, M.B.S, B.F.P, and M.D.W; Software, P.M.H and L.A.M; Validation, P.M.H, L.A.M; Formal Analysis, P.M.H, L.A.M, and M.D.W; Investigation, P.M.H and L.A.M; Resources, L.B, M.B.S, and B.F.P; Data Curation, P.M.H and L.A.M; Writing – Original Draft, P.M.H and M.D.W; Writing – Review & Editing, P.M.H, L.A.M, B.F.P and M.D.W; Visualization, P.M.H. and M.D.W.; Supervision, M.D.W.; Project Administration, M.D.W.; Funding Acquisition, M.D.W.

Competing interest statement

The authors declare no competing financial interests.

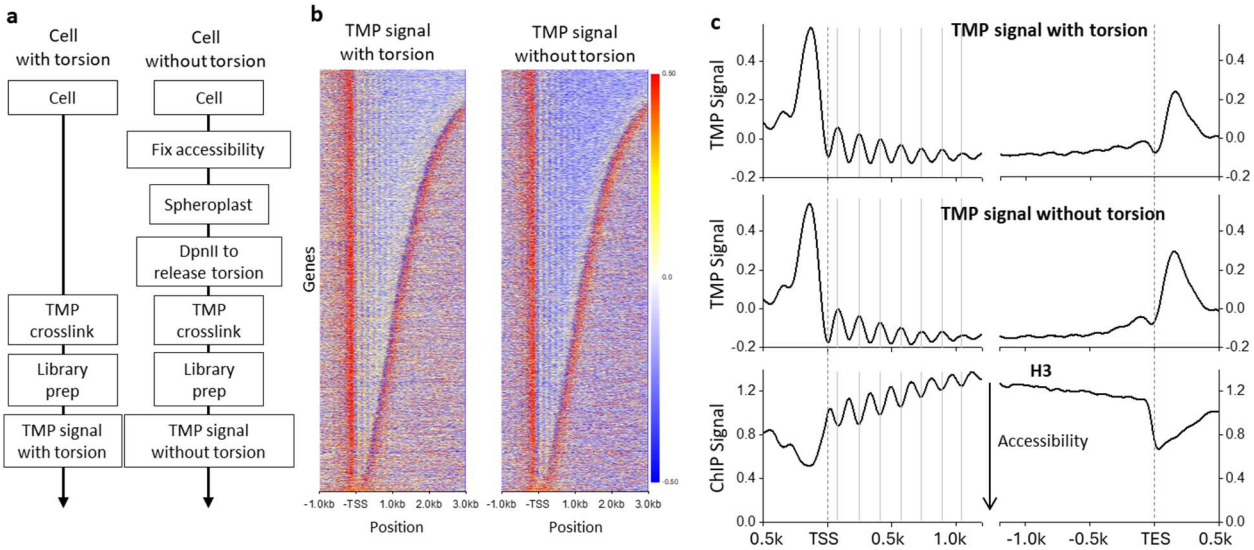

Figure 1. Measurement of the zero-torsion TMP baseline.

(a) Strategy for determination of the TMP signal with and without torsion. (left) Cells with torsion are crosslinked with TMP prior to library preparation for the TMP signal measurement. (right) To measure the TMP baseline signal without torsion, the native-bound protein landscape is fixed by formaldehyde, and the torsion is released via DpnII digestion of the spheroplast cells before TMP crosslinking. Both TMP crosslinking samples are then mapped using Illumina-based sequencing to generate the TMP signal (Materials and Methods).

(b) Heatmaps of TMP signals aligned at the TSSs of 5,925 genes for both the TMP signal with torsion (left, n = 2 biological replicates) and the TMP signal without torsion (right, n = 3 biological replicates) with rows sorted by the ORF size. The TMP signal was normalized against that of the purified DNA.

(c) (top) Average TMP signals with and without torsion from data in (b) aligned at the TSS (left) and aligned at the TES (right). For comparison, previous H3-ChIP-MNase-Seq data[27] are also shown (bottom). To minimize signal bias from neighboring genes, signals downstream of the TES were excluded from the analysis of the left panel plots, and signals upstream of the TTS were excluded from the analysis of the right panel plots.

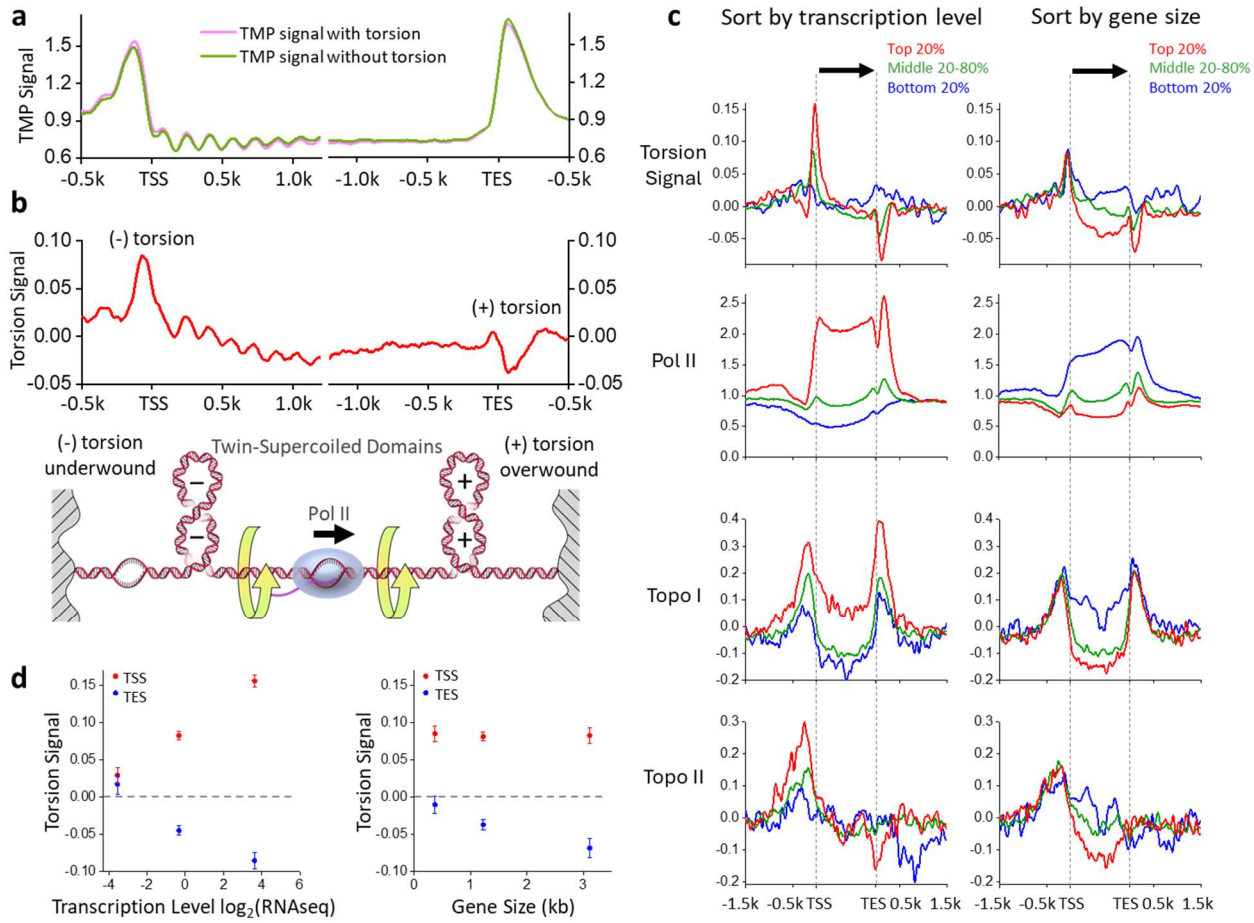

Figure 2. The twin-supercoiled domains of transcription.

(a) Average TMP signals with and without torsion using data from Fig. 1c, replotted for easy comparison, except without normalization against that of the purified DNA.

(b) The torsion signal, defined as the difference between the TMP signal with torsion and the TMP signal without torsion. The bottom cartoon shows the twin-supercoiled domain model of transcription.

(c) The torsion signal of genes sorted by transcription level and gene size, with genes grouped by percentiles of mRNA abundance and ORF size, respectively. Positions within the gene body are scaled by the gene length while preserving the torsion signal amplitude (Materials and Methods). The torsion signal is compared to previous data of Pol II (Rpb3-ChIP-Exo)[27], topo I (Top1-ChIP-Exo)[27], and topo II (Top2-ChIP Exo)[27].

(d) Mean value of the torsion signal averaged within 20 bp of either the peak near the TSS (red) or the valley near the TES (blue) as functions of the average gene expression level (left) or gene size (right) within the percentile groups specified in (c). Error bars are standard errors of the means.

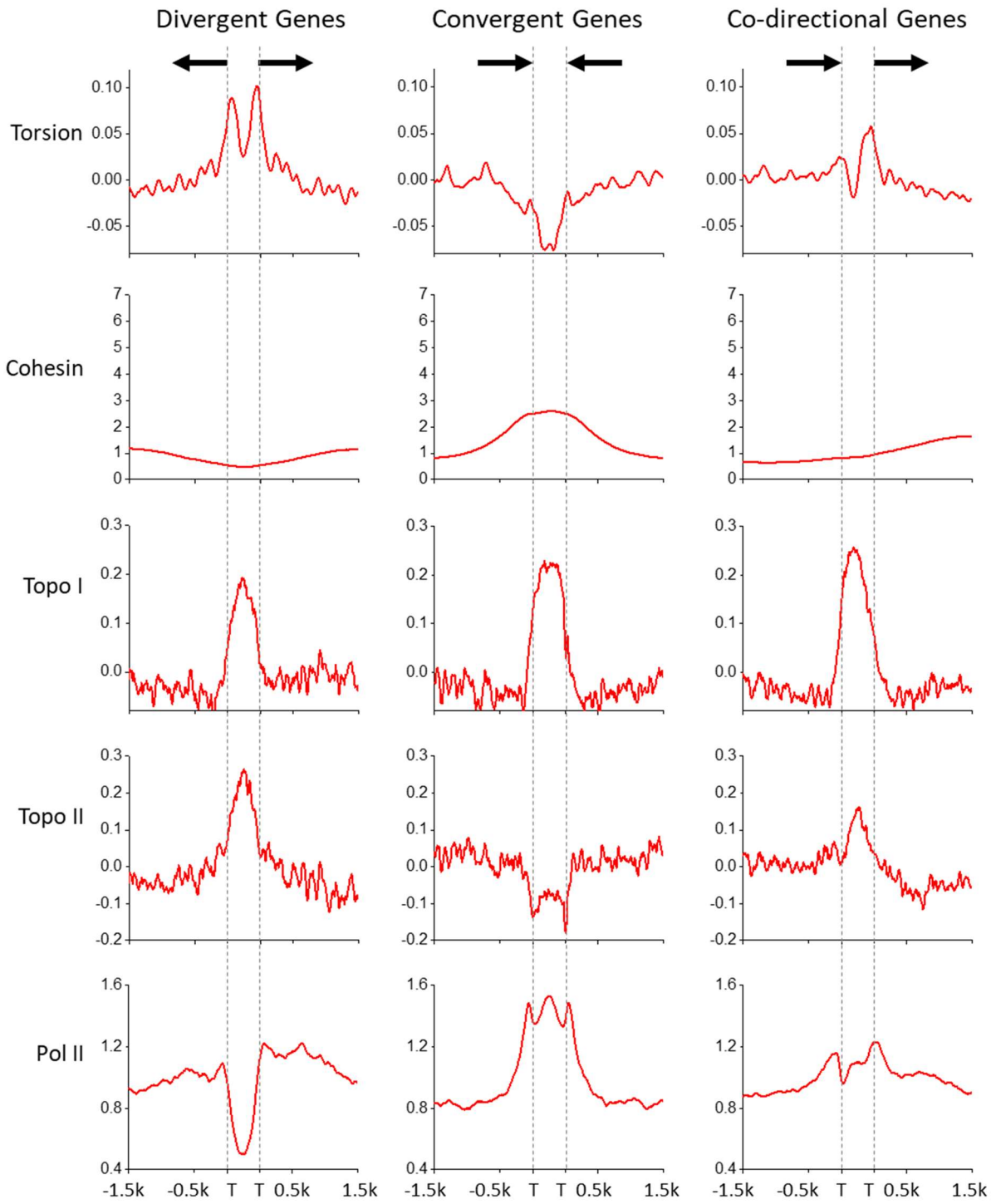

Figure 3. Torsion between genes. The torsion signal plotted for three gene-pair configurations: divergent (left, 1275 pairs), convergent (middle, 1364 pairs), co-directional (right, 2426 pairs). The torsion signal is compared to previous protein mapping data of the same gene-pair configurations for cohesin (SccI-Chip)[24], topo I (Top1-ChIP-Exo)[27], and topo II (Top2-ChIP Exo)[27], and Pol II (Rpb3-ChIP-Exo)[27]. TSS or TES is indicated as "T".

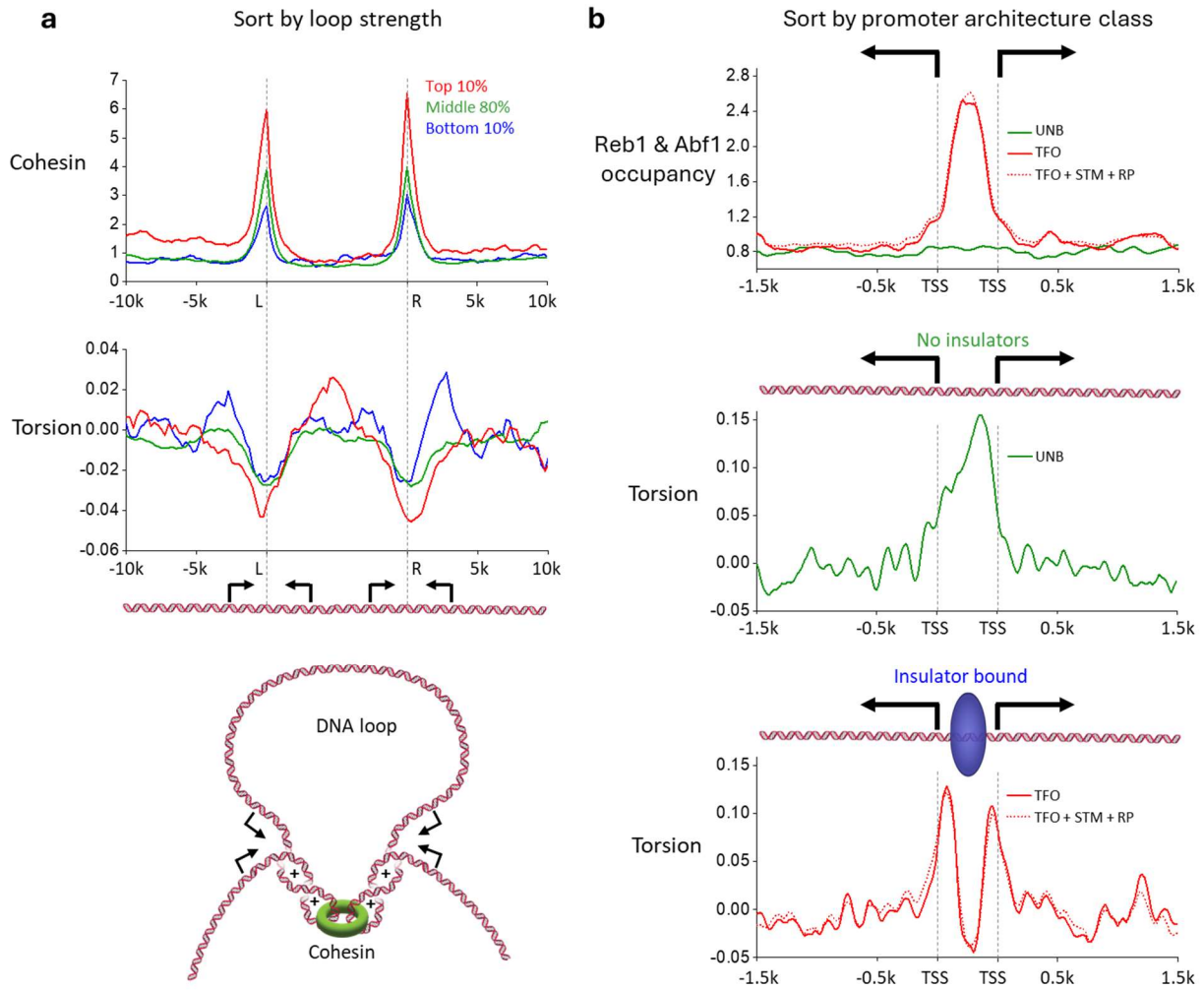

517

518 **Figure 4. Torsion impacts 3D genome structure and couples gene expression.**

519 (a) Cohesin-ChIP seq[24] and torsion signals plotted across 527 detected mitotic loops from
520 previous MicroC-XL Data[52], grouped by percentiles of the loop score. Positions between the two
521 loop boundaries (L and R) are scaled by the DNA length between the boundaries while
522 preserving the torsion signal amplitude (Materials and Methods). Below is a cartoon depicting a
523 DNA loop anchored by cohesin at sites of (+) supercoiling.

524 (b) Average ChIP-Exo signal of Abf1 and Reb1[27] (top plot), and torsion plotted across subsets of
525 divergent genes (middle and bottom plots). Gene pairs are separated by defined classes[27]
526 where both genes in the pair are of the same class as follows: unbound class (UNB; green, 421
527 pairs), ssTFs only (TFO; red-solid, 320 pairs), ssTFs and other factors (TFO, STM, and RP; red-
528 dotted, 439 pairs). Positions between the two divergent promoters are scaled by DNA length
529 between the two promoters while preserving the signal amplitude (Materials and Methods).

530

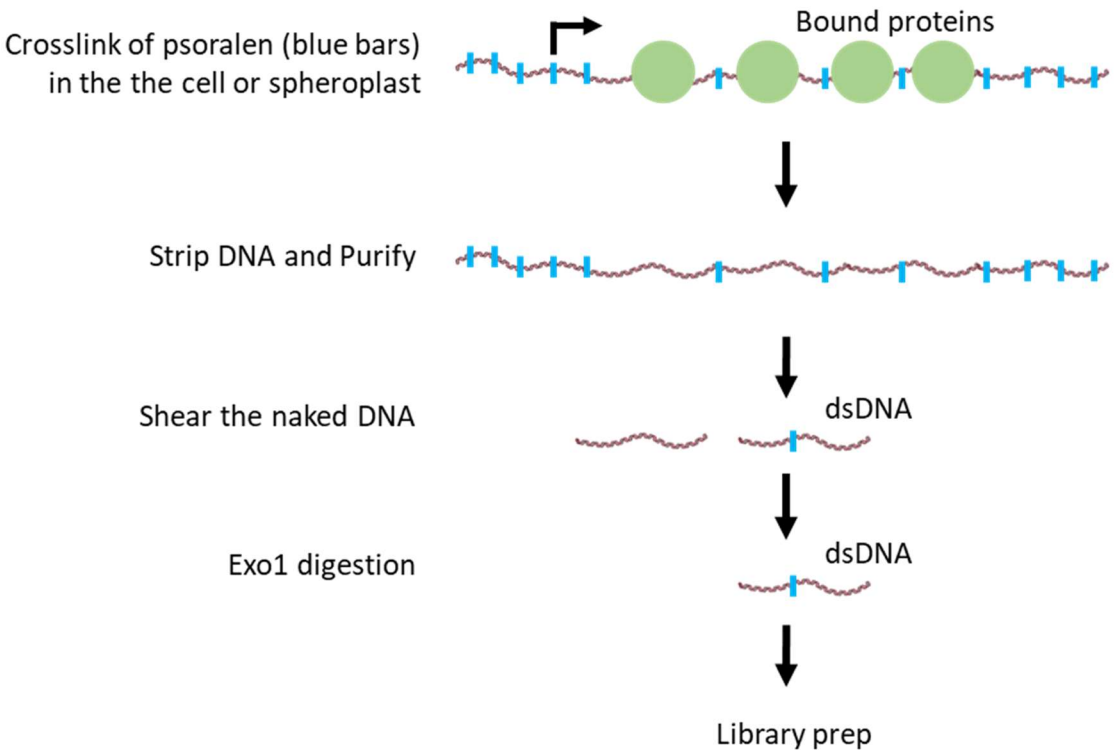

Figure Supplement 1. Psoralen binding and accessibility. Cartoon depicting the experimental method for mapping TMP cross-linking on genomic DNA. The TMP has preferential binding to naked DNA where there are no bound proteins, such as in nucleosome-free regions and on linker DNA.

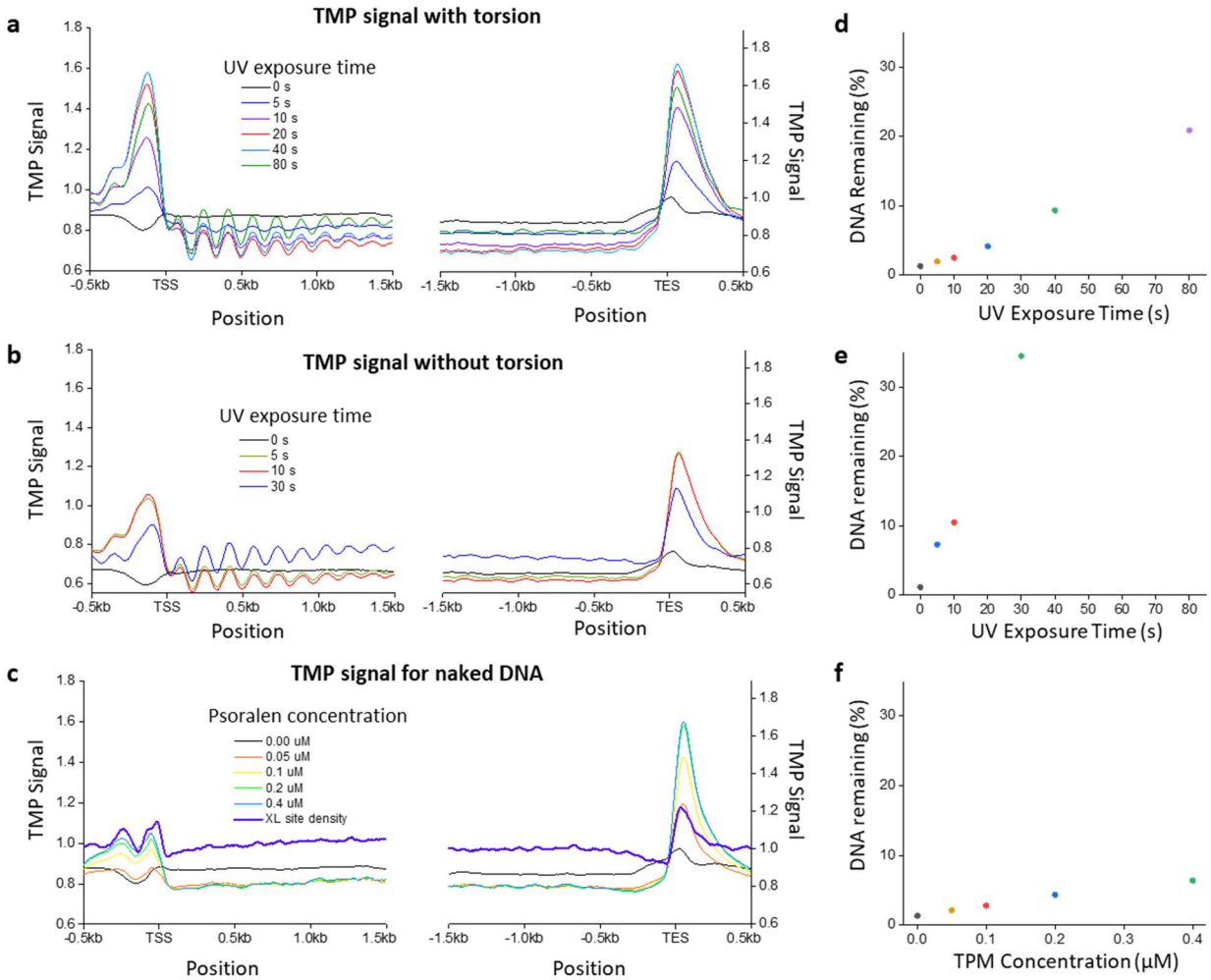

Figure Supplement 2. Psoralen Crosslinking Conditions.

(a) Average TMP signal with torsion of all 5925 genes as in Figure 1, shown for increasing UV dosage on cells. (Porter: did you divide by the purified DNA signal?)

(b) Average TMP signal without torsion from the same genes.

(c) Average TMP signal of naked genomic DNA from the same genes. 250 ng of sheared naked genomic DNA was incubated for 2 min with the indicated concentration of psoralen and exposed to UV light for 10 s. The density of adjacent AT or TA dinucleotide cross-linking sites is plotted for comparison with the naked DNA profiles (XL site density, dark blue).

(d-f) Percent of 250 ng of input DNA remaining after two rounds of denaturation and treatment with ExoI for each respective condition in (a-c). The response in % DNA remaining is near linear with UV dosage. At low concentrations, we see that the % DNA remaining approaches the background (d-f) as does the signal from the library prep (a-c). This indicates that if the dose is

too low, the signal-to-noise limit is being approached. Upon high UV exposure, the % DNA remaining indicates that there are likely multiple crosslinks/fragments (d,e), which may lead to artifacts due to the loss of small fragments during library prep. Upon a Goldilocks dose of UV exposure or psoralen concentration, signals are very similar to each other, indicating that most fragments have exactly one crosslink after Exo digestion (Fig. Supplement 3).

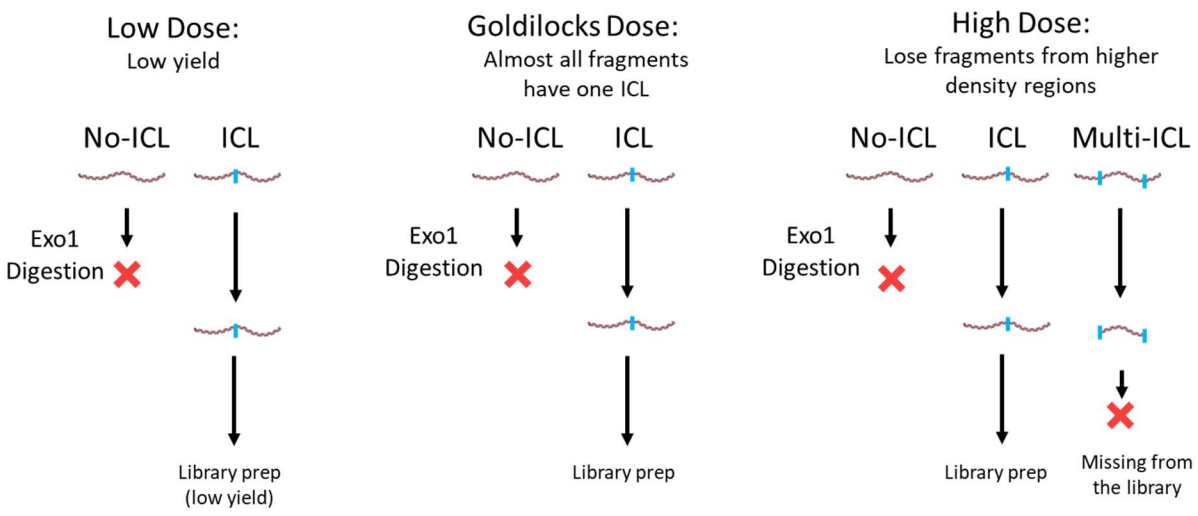

Figure Supplement 3. Optimal TMP crosslinking density. Cartoon depicting the optimal inter-strand cross-linking density is when each fragment of DNA has only one TMP cross-link after Exonuclease I digestion.

575 ## References
576

577 (1) Liu, L. F.; Wang, J. C. Supercoiling of the DNA Template during Transcription. *Proceedings of the*
578 *National Academy of Sciences of the United States of America* **1987**, *84*, 7024–7027.
579 (2) Ma, J.; Bai, L.; Wang, M. D. Transcription under Torsion. *Science* **2013**, *340*, 1580–1583.
580 (3) Ma, J.; Tan, C.; Gao, X.; Fulbright, R. M.; Roberts, J. W.; Wang, M. D. Transcription Factor
581 Regulation of RNA Polymerase's Torque Generation Capacity. *Biophysical Journal* **2019**, *116* (3),
582 210a.
583 (4) Wu, H.-Y.; Shyy, S.; Wang, J. C.; Liu, L. F. Transcription Generates Positively and Negatively
584 Supercoiled Domains in the Template. *Cell* **1988**, *53* (3), 433–440.
585 (5) Kouzine, F.; Liu, J.; Sanford, S.; Chung, H.-J.; Levens, D. The Dynamic Response of Upstream DNA to
586 Transcription-Generated Torsional Stress. *Nature structural & molecular biology* **2004**, *11* (11),
587 1092–1100.
588 (6) Kouzine, F.; Sanford, S.; Elisha-Feil, Z.; Levens, D. The Functional Response of Upstream DNA to
589 Dynamic Supercoiling in Vivo. *Nature structural & molecular biology* **2008**, *15* (2), 146–154.
590 (7) Kim, S.; Beltran, B.; Irnov, I.; Jacobs-Wagner, C. Long-Distance Cooperative and Antagonistic RNA
591 Polymerase Dynamics via DNA Supercoiling. *Cell* **2019**, *179* (1), 106-119. e16.
592 (8) Wang, J. C. Interaction between DNA and an Escherichia Coli Protein ω. *Journal of molecular*
593 *biology* **1971**, *55* (3), 523-IN16.
594 (9) Wang, J. C. Cellular Roles of DNA Topoisomerases: A Molecular Perspective. *Nature reviews*
595 *Molecular cell biology* **2002**, *3* (6), 430–440.
596 (10) Nitiss, J. L. Investigating the Biological Functions of DNA Topoisomerases in Eukaryotic Cells.
597 *Biochimica et Biophysica Acta (BBA)-Gene Structure and Expression* **1998**, *1400* (1–3), 63–81.
598 (11) Pommier, Y.; Nussenzweig, A.; Takeda, S.; Austin, C. Human Topoisomerases and Their Roles in
599 Genome Stability and Organization. *Nature reviews Molecular cell biology* **2022**, *23* (6), 407–427.
600 (12) Lee, J. H.; Berger, J. M. Cell Cycle-Dependent Control and Roles of DNA Topoisomerase II. *Genes*
601 **2019**, *10* (11), 859.
602 (13) Wu, M.; Beck, C.; Lee, J. H.; Fulbright, R. M.; Jeong, J.; Inman, J. T.; Woodhouse, M. V.; Berger, J.
603 M.; Wang, M. D. Human Topoisomerase IIα Promotes Chromatin Condensation Via a Phase
604 Transition. bioRxiv October 18, 2024, p 2024.10.15.618281.
605 https://doi.org/10.1101/2024.10.15.618281.
606 (14) Qian, J.; Lubkowska, L.; Zhang, S.; Tan, C.; Hong, Y.; Fulbright, R. M.; Inman, J. T.; Kay, T. M.; Jeong,
607 J.; Gotte, D.; Berger, J. M.; Kashlev, M.; Wang, M. D. Chromatin Buffers Torsional Stress During
608 Transcription. bioRxiv October 18, 2024, p 2024.10.15.618270.
609 https://doi.org/10.1101/2024.10.15.618270.
610 (15) Bermejo, R.; Doksani, Y.; Capra, T.; Katou, Y.-M.; Tanaka, H.; Shirahige, K.; Foiani, M. Top1-and
611 Top2-Mediated Topological Transitions at Replication Forks Ensure Fork Progression and Stability
612 and Prevent DNA Damage Checkpoint Activation. *Genes & development* **2007**, *21* (15), 1921–1936.
613 (16) Pommier, Y.; Sun, Y.; Huang, S. N.; Nitiss, J. L. Roles of Eukaryotic Topoisomerases in Transcription,
614 Replication and Genomic Stability. *Nature reviews Molecular cell biology* **2016**, *17* (11), 703–721.
615 (17) Sheinin, M. Y.; Forth, S.; Marko, J. F.; Wang, M. D. Underwound DNA under Tension: Structure,
616 Elasticity, and Sequence-Dependent Behaviors. *Physical review letters* **2011**, *107* (10), 108102.
617 (18) Gao, X.; Hong, Y.; Ye, F.; Inman, J. T.; Wang, M. D. Torsional Stiffness of Extended and Plectonemic
618 DNA. *Phys. Rev. Lett.* **2021**, *127* (2), 028101. https://doi.org/10.1103/PhysRevLett.127.028101.
619 (19) Hong, Y.; Park, S. ha; Wang, H.; Wang, M. D. Geometry of Braided DNA Dictates Supercoiling
620 Partition. bioRxiv October 11, 2024, p 2024.10.08.617221.
621 https://doi.org/10.1101/2024.10.08.617221.

622 (20) Singh, G.; Hong, Y.; Inman, J. T.; Sethna, J. P.; Wang, M. D. Torsional Mechanics of Circular DNA.
623 *bioRxiv* **2024**, 2024.10.08.617281. https://doi.org/10.1101/2024.10.08.617281.
624 (21) Jia, X.; Gao, X.; Zhang, S.; Inman, J. T.; Hong, Y.; Singh, A.; Patel, S.; Wang, M. D. Torsion Is a
625 Dynamic Regulator of DNA Replication Stalling and Reactivation. bioRxiv October 17, 2024, p
626 2024.10.14.618227. https://doi.org/10.1101/2024.10.14.618227.
627 (22) Sheinin, M. Y.; Li, M.; Soltani, M.; Luger, K.; Wang, M. D. Torque Modulates Nucleosome Stability
628 and Facilitates H2A/H2B Dimer Loss. *Nature communications* **2013**, *4* (1), 2579.
629 (23) Jeppsson, K.; Sakata, T.; Nakato, R.; Milanova, S.; Shirahige, K.; Björkegren, C. Cohesin-Dependent
630 Chromosome Loop Extrusion Is Limited by Transcription and Stalled Replication Forks. *Science*
631 *Advances* **2022**, *8*.
632 (24) Jeppsson, K.; Pradhan, B.; Sutani, T.; Sakata, T.; Igarashi, M. U.; Berta, D. G.; Kanno, T.; Nakato, R.;
633 Shirahige, K.; Kim, E. Loop-Extruding Smc5/6 Organizes Transcription-Induced Positive DNA
634 Supercoils. *Molecular Cell* **2024**, *84* (5), 867-882. e5.
635 (25) Racko, D.; Benedetti, F.; Dorier, J.; Stasiak, A. Are TADs Supercoiled? *Nucleic acids research* **2019**,
636 *47* (2), 521–532.
637 (26) Johnstone, C. P.; Galloway, K. E. Supercoiling-Mediated Feedback Rapidly Couples and Tunes
638 Transcription. *Cell Reports* **2022**, *41* (3). https://doi.org/10.1016/j.celrep.2022.111492.
639 (27) Rossi, M. J.; Kuntala, P. K.; Lai, W. K. M.; Yamada, N.; Badjatia, N.; Mittal, C.; Kuzu, G.; Bocklund, K.;
640 Farrell, N. P.; Blanda, T. R.; Mairose, J. D.; Basting, A. V.; Mistretta, K. S.; Rocco, D. J.; Perkinson, E.
641 S.; Kellogg, G. D.; Mahony, S.; Pugh, B. F. A High-Resolution Protein Architecture of the Budding
642 Yeast Genome. *Nature* **2021**, *592*, 309–314.
643 (28) Yan, C.; Zhang, D.; Raygoza Garay, J. A.; Mwangi, M. M.; Bai, L. Decoupling of Divergent Gene
644 Regulation by Sequence-Specific DNA Binding Factors. *Nucleic Acids Research* **2015**, *43* (15), 7292–
645 7305. https://doi.org/10.1093/nar/gkv618.
646 (29) Thazhathveetil, A. K.; Liu, S.-T.; Indig, F. E.; Seidman, M. M. Psoralen Conjugates for Visualization of
647 Genomic Interstrand Cross-Links Localized by Laser Photoactivation. *Bioconjugate chemistry* **2007**,
648 *18* (2), 431–437.
649 (30) Bermúdez, I.; García-Martínez, J.; Pérez-Ortín, J. E.; Roca, J. A Method for Genome-Wide Analysis
650 of DNA Helical Tension by Means of Psoralen-DNA Photobinding. *Nucleic Acids Res* **2010**.
651 (31) Sinden, R. R.; Carlson, J. O.; Pettijohn, D. E. Torsional Tension in the DNA Double Helix Measured
652 with Trimethylpsoralen in Living E. Coli Cells: Analogous Measurements in Insect and Human Cells.
653 *Cell* **1980**, *21* (3), 773–783.
654 (32) Kouzine, F.; Gupta, A.; Baranello, L.; Wojtowicz, D.; Ben-Aissa, K.; Liu, J.; Przytycka, T.; Levens, D.
655 Transcription-Dependent Dynamic Supercoiling Is a Short-Range Genomic Force. *Nature Structural*
656 *and Molecular Biology* **2013**, *20*, 396–403.
657 (33) Teves, S. S.; Henikoff, S. Transcription-Generated Torsional Stress Destabilizes Nucleosomes.
658 *Nature structural & molecular biology* **2014**, *21*, 88–94.
659 (34) Naughton, C.; Avlonitis, N.; Corless, S.; Prendergast, J.; MAti, I.; Eijk, P.; Cockroft, S.; Bradley, M.;
660 Ylstra, B.; Gilbert, N. Transcription Forms and Remodels Supercoiling Domains Unfolding Large-
661 Scale Chromatin Structures. *Nature Structural and Molecular Biology* **2013**, *20*, 387–395.
662 (35) Yao, Q.; Zhu, L.; Shi, Z.; Banerjee, S.; Chen, C. Topoisomerase-Modulated Genome-Wide DNA
663 Supercoiling Domains Colocalize with Nuclear Compartments and Regulate Human Gene
664 Expression. (). *Nature structural & molecular biology* **2024**.
665 (36) Achar, Y. J.; Adhil, M.; Choudhary, R.; Gilbert, N.; Foiani, M. Negative Supercoil at Gene Boundaries
666 Modulates Gene Topology. *Nature* **2020**, *577*, 701–705.
667 (37) Jiang, C.; Pugh, B. F. Nucleosome Positioning and Gene Regulation: Advances through Genomics.
668 *Nature Reviews Genetics* **2009**, *10* (3), 161–172.

669 (38) Mavrich, T. N.; Ioshikhes, I. P.; Venters, B. J.; Jiang, C.; Tomsho, L. P.; Qi, J.; Schuster, S. C.; Albert, I.;
670 Pugh, B. F. A Barrier Nucleosome Model for Statistical Positioning of Nucleosomes throughout the
671 Yeast Genome. *Genome research* **2008**, *18* (7), 1073–1083.
672 (39) Booth, G. T.; Wang, I. X.; Cheung, V. G.; Lis, J. T. Divergence of a Conserved Elongation Factor and
673 Transcription Regulation in Budding and Fission Yeast. *Genome research* **2016**, *26* (6), 799–811.
674 (40) Chong, S.; Chen, C.; Ge, H.; Xie, X. S. Mechanism of Transcriptional Bursting in Bacteria. *Cell* **2014**,
675 *158* (2), 314–326.
676 (41) Giaever, G. N.; Wang, J. C. Supercoiling of Intracellular DNA Can Occur in Eukaryotic Cells. *Cell*
677 **1988**, *55* (5), 849–856.
678 (42) Brill, S. J.; DiNardo, S.; Voelkel-Meiman, K.; Sternglanz, R. Need for DNA Topoisomerase Activity as
679 a Swivel for DNA Replication for Transcription of Ribosomal RNA. *Nature* **1987**, *326* (6111), 414–
680 416.
681 (43) Champoux, J. J. DNA Topoisomerases: Structure, Function, and Mechanism. *Annual review of*
682 *biochemistry* **2001**, *70* (1), 369–413.
683 (44) Lee, J.; Wu, M.; Inman, J. T.; Singh, G.; Park, S. H.; Lee, J. H.; Fulbright, R. M.; Hong, Y.; Jeong, J.;
684 Berger, J. M. Chromatinization Modulates Topoisomerase II Processivity. *Nature communications*
685 **2023**, *14* (1), 6844.
686 (45) Le, T. T.; Wu, M.; Lee, J. H.; Bhatt, N.; Inman, J. T.; Berger, J. M.; Wang, M. D. Etoposide Promotes
687 DNA Loop Trapping and Barrier Formation by Topoisomerase II. *Nature chemical biology* **2023**, *19*
688 (5), 641–650.
689 (46) Roca, J.; Wang, J. C. DNA Transport by a Type II DNA Topoisomerase: Evidence in Favor of a Two-
690 Gate Mechanism. *Cell* **1994**, *77* (4), 609–616.
691 (47) Berger, J. M.; Gamblin, S. J.; Harrison, S. C.; Wang, J. C. Structure and Mechanism of DNA
692 Topoisomerase II. *Nature* **1996**, *379* (6562), 225–232.
693 (48) Le, T. T.; Gao, X.; ha Park, S.; Lee, J.; Inman, J. T.; Lee, J. H.; Killian, J. L.; Badman, R. P.; Berger, J. M.;
694 Wang, M. D. Synergistic Coordination of Chromatin Torsional Mechanics and Topoisomerase
695 Activity. *Cell* **2019**, *179* (3), 619-631. e15.
696 (49) Bancaud, A.; Wagner, G.; e Silva, N. C.; Lavelle, C.; Wong, H.; Mozziconacci, J.; Barbi, M.; Sivolob,
697 A.; Le Cam, E.; Mouawad, L. Nucleosome Chiral Transition under Positive Torsional Stress in Single
698 Chromatin Fibers. *Molecular Cell* **2007**, *27* (1), 135–147.
699 (50) Bermejo, R.; Lai, M. S.; Foiani, M. Preventing Replication Stress to Maintain Genome Stability:
700 Resolving Conflicts between Replication and Transcription. *Molecular Cell* **2012**, *45* (6), 710–718.
701 https://doi.org/10.1016/j.molcel.2012.03.001.
702 (51) Patel, H. P.; Coppola, S.; Pomp, W.; Aiello, U.; Brouwer, I.; Libri, D.; Lenstra, T. L. DNA Supercoiling
703 Restricts the Transcriptional Bursting of Neighboring Eukaryotic Genes. *Molecular Cell* **2023**, *83*
704 (10), 1573-1587. e8.
705 (52) Costantino, L.; Hsieh, T. H. S.; Lamothe, R.; Darzacq, X.; Koshland, D. Cohesin Residency Determines
706 Chromatin Loop Patterns. *eLife* **2020**, *9*, 1–31.
707 (53) Candelli, T.; Challal, D.; Briand, J.; Boulay, J.; Porrua, O.; Colin, J.; Libri, D. High-resolution
708 Transcription Maps Reveal the Widespread Impact of Roadblock Termination in Yeast. *The EMBO*
709 *Journal* **2018**, *37* (4), e97490. https://doi.org/10.15252/embj.201797490.
710 (54) Ganapathi, M.; Palumbo, M. J.; Ansari, S. A.; He, Q.; Tsui, K.; Nislow, C.; Morse, R. H. Extensive Role
711 of the General Regulatory Factors, Abf1 and Rap1, in Determining Genome-Wide Chromatin
712 Structure in Budding Yeast. *Nucleic Acids Research* **2011**, *39* (6), 2032–2044.
713 https://doi.org/10.1093/nar/gkq1161.
714 (55) Wu, A. C. K.; Patel, H.; Chia, M.; Moretto, F.; Frith, D.; Snijders, A. P.; Werven, F. J. van. Repression
715 of Divergent Noncoding Transcription by a Sequence-Specific Transcription Factor. *Molecular Cell*
716 **2018**, *72* (6), 942-954.e7. https://doi.org/10.1016/j.molcel.2018.10.018.

(56) Cesur, M. F.; Çakır, T.; Pir, P. Genome-Wide Analysis of Yeast Metabolic Cycle through Metabolic Network Models Reveals Superiority of Integrated ATAC-Seq Data over RNA-Seq Data. *Msystems* **2022**, *7* (3), e01347-21.
(57) Guo, M. S.; Kawamura, R.; Littlehale, M. L.; Marko, J. F.; Laub, M. T. High-Resolution, Genome-Wide Mapping of Positive Supercoiling in Chromosomes. *eLife* **2021**, *10*, e67236.
(58) Viggiani, C. J.; Aparicio, O. M. New Vectors for Simplified Construction of BrdU-Incorporating Strains of Saccharomyces Cerevisiae. *Yeast* **2006**, *23* (14–15), 1045–1051. https://doi.org/10.1002/yea.1406.
(59) Vasimuddin, M.; Misra, S.; Li, H.; Aluru, S. Efficient Architecture-Aware Acceleration of BWA-MEM for Multicore Systems; IEEE, 2019; pp 314–324.
(60) Danecek, P.; Bonfield, J. K.; Liddle, J.; Marshall, J.; Ohan, V.; Pollard, M. O.; Whitwham, A.; Keane, T.; McCarthy, S. A.; Davies, R. M. Twelve Years of SAMtools and BCFtools. *Gigascience* **2021**, *10* (2), giab008.
(61) *Picard Tools*.
(62) Ramírez, F.; Ryan, D. P.; Grüning, B.; Bhardwaj, V.; Kilpert, F.; Richter, A.; Heyne, S.; Dündar, F.; Manke, T. deepTools2: A next Generation Web Server for Deep-Sequencing Data Analysis. *Nucleic Acids Research* **2016**, *44*, W160–W165.
(63) Raney, B. J.; Barber, G. P.; Benet-Pagès, A.; Casper, J.; Clawson, H.; Cline, M. S.; Diekhans, M.; Fischer, C.; Navarro Gonzalez, J.; Hickey, G. The UCSC Genome Browser Database: 2024 Update. *Nucleic acids research* **2024**, *52* (D1), D1082–D1088.
(64) Cherry, J. M.; Hong, E. L.; Amundsen, C.; Balakrishnan, R.; Binkley, G.; Chan, E. T.; Christie, K. R.; Costanzo, M. C.; Dwight, S. S.; Engel, S. R. Saccharomyces Genome Database: The Genomics Resource of Budding Yeast. *Nucleic acids research* **2012**, *40* (D1), D700–D705.
(65) Sayers, E. W.; Bolton, E. E.; Brister, J. R.; Canese, K.; Chan, J.; Comeau, D. C.; Connor, R.; Funk, K.; Kelly, C.; Kim, S. Database Resources of the National Center for Biotechnology Information. *Nucleic acids research* **2022**, *50* (D1), D20–D26.
(66) Open2C; Abdennur, N.; Abraham, S.; Fudenberg, G.; Flyamer, I. M.; Galitsyna, A. A.; Goloborodko, A.; Imakaev, M.; Oksuz, B. A.; Venev, S. V. Cooltools: Enabling High-Resolution Hi-C Analysis in Python. *PLOS Computational Biology* **2024**, *20* (5), e1012067.